ChemBioChem

Research Article
doi.org/10.1002/cbic.202400064

Chemistry Europe
European Chemical Societies Publishing

www.chembiochem.org

Biological Demands and Toxicity of Isoprenoid Precursors in Bacillus Subtilis Through Cell-Permeant Analogs of Isopentenyl Pyrophosphate and Dimethylallyl Pyrophosphate

Dillon P. McBee,[a] Zackary N. Hulsey,[a] Makayla R. Hedges,[a] and Joshua A. Baccile*[a]

Bacterial isoprenoids are necessary for many biological processes, including maintaining membrane integrity, facilitating intercellular communication, and preventing oxidative damage. All bacterial isoprenoids are biosynthesized from two five carbon structural isomers, isopentenyl pyrophosphate (IPP) and dimethylallyl pyrophosphate (DMAPP), which are cell impermeant. Herein, we demonstrate exogenous delivery of IPP and DMAPP into *Bacillus subtilis* by utilizing a self-immolative ester (SIE)-caging approach. We initially evaluated native *B. subtilis* esterase activity, which revealed a preference for short straight chain esters. We then examined the viability of the SIE-caging approach in *B. subtilis* and demonstrate that the released caging groups are well tolerated and the released IPP and DMAPP are bioavailable, such that isoprenoid biosynthesis can be rescued in the presence of pathway inhibitors. We further show that IPP and DMAPP are both toxic and inhibit growth of *B. subtilis* at the same concentration. Lastly, we establish the optimal ratio of IPP to DMAPP (5:1) for *B. subtilis* growth and find that, surprisingly, DMAPP alone is insufficient to rescue isoprenoid biosynthesis under high concentrations of fosmidomycin. These findings showcase the potential of the SIE-caging approach in *B. subtilis* and promise to both aid in novel isoprenoid discovery and to inform metabolic engineering efforts in bacteria.

Introduction

Isoprenoids are critical for cellular physiology due to their roles in protein prenylation, cellular oxidative control, membrane stability, and small-molecule signaling. Regardless of the organism, the biosynthesis of all isoprenoids proceeds from two central five-carbon isomers, isopentenyl pyrophosphate (IPP) and dimethylallyl pyrophosphate (DMAPP), which are condensed in a head-to-tail fashion to form the skeletal backbone of all longer chain isoprenoids.[1,2] In eukaryotes and prokaryotes, IPP and DMAPP are produced through either the mevalonic acid pathway (MVA) or the methyl-erythritol phosphate (MEP) pathway, respectively.[3,4] The MVA pathway, used by mammalian cells, proceeds through several enzymatic steps starting from two molecules of acetyl-CoA, producing IPP that is then converted to DMAPP via the isopentenyl pyrophosphate isomerase (IPPI).[5–7] Conversely, prokaryotes predominantly utilize the MEP pathway, in which both IPP and DMAPP are simultaneously produced from pyruvate and glyceraldehyde-3-phosphate without the need for IPPI isomerization to produce both required substrates for downstream isoprenoid biosynthesis (Figure 1A).[8,9]

The biosynthesis and regulation of isoprenoids in humans has been of immense interest primarily due to the importance of cholesterol and hormones, as well as protein prenylation, a post-translational modification that is necessary for normal function and transport of many growth factors (e.g., Ras, Rab, and Rho families).[10,11] Historically, plants and fungi were the main focus for the discovery of new isoprenoids; however, more than 1,000 bacterial isoprenoids have been characterized across 55 subfamilies of natural products to date, with many cryptic isoprenoid biosynthetic gene clusters (BGCs) awaiting characterization.[12] Some notable examples of bacterial isoprenoids include geosmin, virantmycin, and platensimycin. Geosmin is a farnesyl pyrophosphate (FPP) sesquiterpenoid derived from actinomycetes, cyanobacteria, and myxobacteria, generates the characteristic smell of soil.[13–14] Virantmycin is a geranyl pyrophosphate (GPP)-based benzastatin derived from *Streptomyces nitrosporeus* known to have antibacterial, antifungal, antiviral, radical scavenging, and neuronal protection properties.[15] Platensimycin, isolated from *Streptomyces platensis*, is a geranylgeranyl pyrophosphate (GGPP) derived diterpenoid, notable for acting as a potent inhibitor of bacterial fatty acid synthesis in *Staphylococcus aureus*.[16] Additionally, isoprenoids distinct to pathogenetic bacteria, such as those produced in *Mycobacterium tuberculosis* (TB) via unique diterpene cyclases provide unique antibacterial targets (Figure 1B).[17–18]

While the characterization of over a thousand bacterial isoprenoids demonstrate the potential of bacteria as rich sources of new chemistry, the process of uncovering these compounds remains challenging. The discovery of bacterially produced isoprenoids are hindered by a lack of specific chemical tools that enable facile detection of novel compounds from this class of natural products.[19] Currently, the majority of newly introduced bacterial isoprenoids are discovered through

[a] D. P. McBee, Z. N. Hulsey, M. R. Hedges, J. A. Baccile
Department of Chemistry, University of Tennessee, Knoxville, TN, United States
E-mail: jbaccile@utk.edu

Supporting information for this article is available on the WWW under https://doi.org/10.1002/cbic.202400064

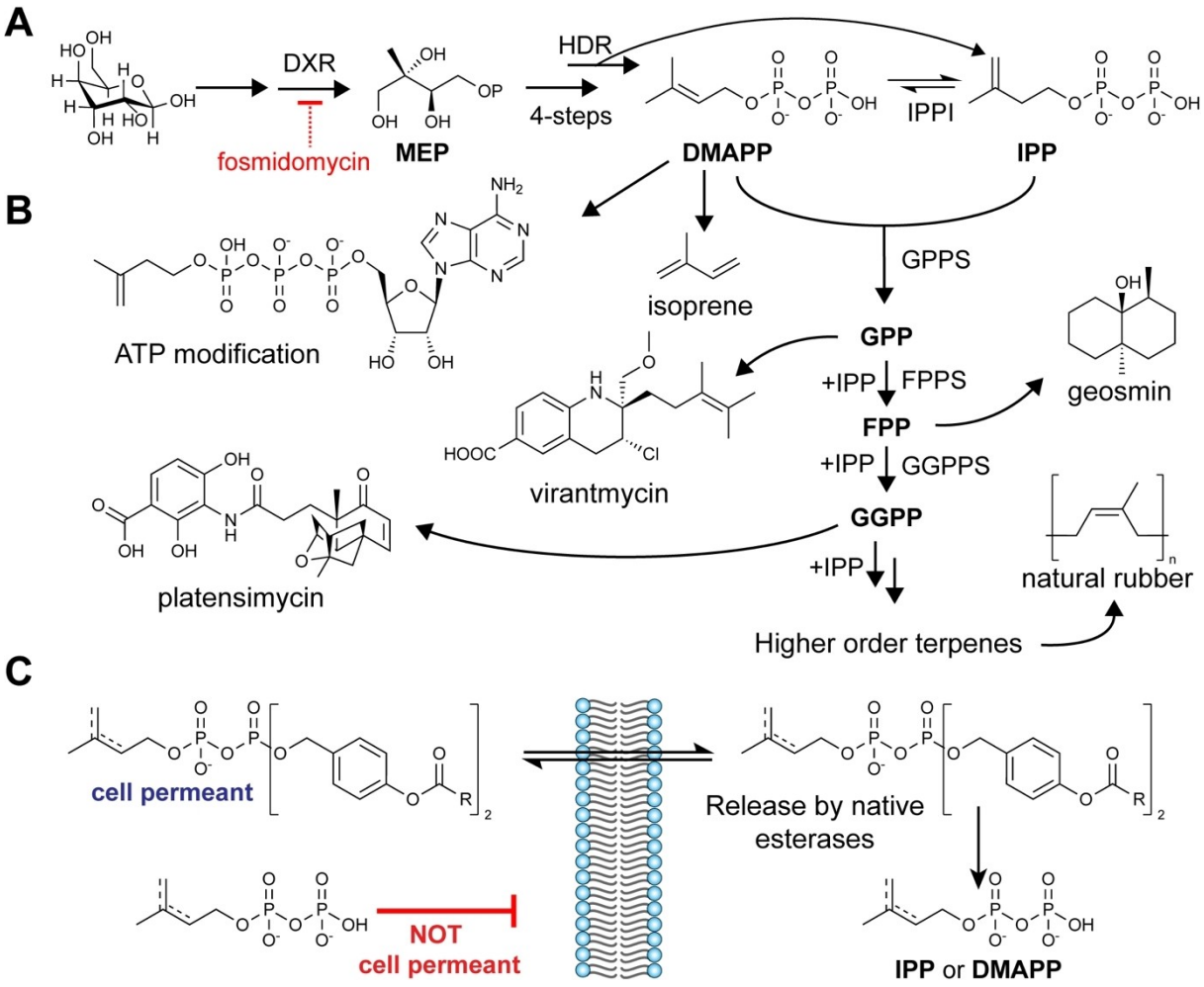

Figure 1. Bacterial isoprenoid biosynthesis and current gap in IPP and DMAPP studies. **(A)** IPP and DMAPP are produced via the MEP pathway in *B. subtilis.* **(B)** IPP and DMAPP form the five-carbon skeleton for a wide range of biologically important small molecules. **(C)** Ester protected β-phosphate of IPP and DMAPP enable membrane permeant delivery of IPP and DMAPP to *B. subtilis.* Abbreviations: MEP – methyl-erythritol phosphate pathway; HDR - (E)-4-hydroxy-3-methylbut-2-enyl diphosphate reductase; FPPS – Farnesyl pyrophosphate synthase; GGPPS – Geranylgeranyl pyrophosphate synthase.

genome mining, which suffers from several fundamental shortcomings.[19,20] For example, putative BGCs are typically identified by sequence similarity with previously identified BGCs, which can potentially lead to the dismissal of new compounds and potential biochemistry. Genome mining approaches are also often restricted to heterologous expression of cryptic BGCs, which is time demanding and, in some cases, simply not possible.[21] Introducing exogenous IPP and DMAPP would facilitate isomer specific compound discovery and enable metabolic enrichment of isoprenoid precursors without the need for genetic engineering.

Beyond the characterization of novel bacterially derived isoprenoids, recent efforts in metabolic engineering have led to the industrial production of the volatile hydrocarbon isoprene in *Bacillus subtilis*, which can act as a potential replacement for fossil fuels or a feedstock for the large-scale production of rubber (Figure 1B).[22–24] The ability to produce isoprene and other commercially or medicinally relevant compounds has been hampered by toxicity resulting from increased expression of MEP pathway enzymes and an increased metabolic flux of IPP or DMAPP, and it is currently unclear if both or one isomer is responsible for the observed toxicity.[25] The current prevailing hypothesis is that the toxicity observed from increased amounts of IPP and DMAPP is caused by off-target production of prenylated adenosine triphosphate (ApppI, Figure 1B).[25,26] The mechanism by which ApppI is generated in bacteria remains elusive.[25] Therefore, a full understanding of the underlying mechanism of toxicity from elevated isoprenoid precursors has the potential to uncover alternative engineering strategies to increase yields without being waylaid by host toxicity.

B. subtilis, a model Gram positive organism, is an excellent candidate for development of chemical tools targeting the isoprenoid pathway in bacteria, given its potential for commercial production of isoprene and usage as a heterologous host for designer terpenes. In this report, we demonstrate cellular delivery of the cell-impermeant isoprenoid precursors, IPP and DMAPP to *B. subtilis* by advancing our previously developed pro-drug like approach using esterase-dependent self-immolative ester (SIE)-caging of the β-phosphate of IPP and DMAPP (Figure 1C).[27] To optimize the applicability of caged pyrophos-

phates released in *B. subtilis*, we first evaluated their native esterase activity and examined potential toxicity resulting from by-products generated through the SIE approach. Then, we tested the bioavailability of cell-permeant analogs of IPP and DMAPP. Finally, we investigated the biological demands and toxicity limits of IPP and DMAPP in an isomer specific manner.

Results and Discussion

Evaluation and Optimization of β-Phosphate Caging of IPP and DMAPP for Application in Gram Positive Bacteria

We previously developed esterase-dependent cell permeant analogs of IPP and DMAPP **1a**–**2b** that were applied to human cancer cell lines (Figure 2); however, bacterial esterase expression is known to be lower than that of mammalian cancer cells. Similarly, bacterial esterases are known to have substrate preferences which differ from mammalian esterases. To investigate this discrepancy, we adapted a *p*-nitrophenyl ester assay to measure the rate of ester cleavage through the conversion of *p*-nitrophenyl ester to *p*-nitrophenol.[28,29] Building upon previous *p*-nitrophenyl ester derivatives, we synthesized a range of straight and branched chain *p*-nitrophenyl esters (Scheme S1). Each *p*-nitrophenyl ester was tested separately in a high-throughput, 96 well plate assay to examine the esterase activity of *B. subtilis* via measurement of absorbance at 400 nm resulting from release of nitrophenol when incubated with a *B. subtilis* culture at a concentration of 10 mM (Figure S1). The same procedure was followed for the *Escherichia coli* strain DH10β, although a Gram negative bacterium, it is known for its lack of esterase activity and thus serving as a negative control. The general esterase activity of *B. subtilis*, in comparison to *E. coli*, is indicated by the increased absorbance resulting from production of *p*-nitrophenol from cleaved *p*-nitrophenyl esters (Figure S1). This assay demonstrated that *B. subtilis* has native esterase expression that makes it a viable host for introducing SIE-caged IPP and DMAPP. It also informed us that an SIE composition consisting of relatively short straight chain esters was likely the best candidate for IPP and DMAPP.

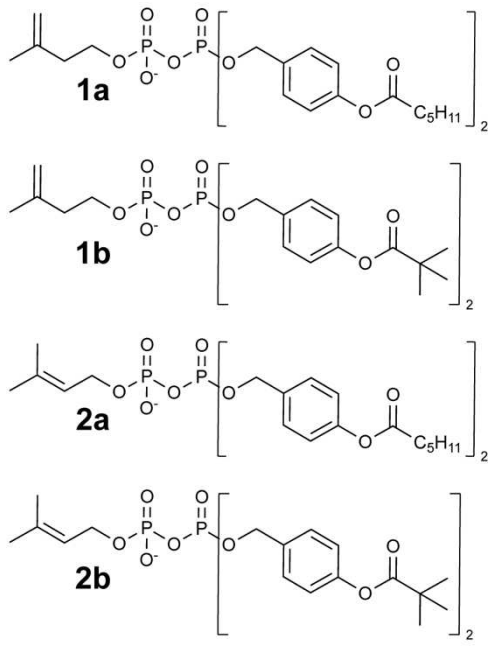

Figure 2. Cell-permeant SIE-caged IPP and DMAPP analogs used in this study.

We then sought to demonstrate that the native esterases of *B. subtilis* could also hydrolyze our SIE-caged IPP and DMAPP. Although the results of the *p*-nitrophenyl ester cleavage assay suggested an acetate ester would allow for the most efficient release of IPP and DMPP, we have demonstrated in past work the low stability of short chain esters in typical growth conditions.[27] We instead balanced stability and ester cleavage by selecting the hexanoate ester (**1a**) and compared it against the pivaloate ester (**1b**), both of which have previously been developed for mammalian cell IPP and DMAPP delivery.[27] To accomplish this, we prepared lysates of *B. subtilis* in Tris buffer at pH 7.5. Next, we added 100 μM of **1a** or **1b** to the lysates, maintained these solutions at 37 °C, and sampled aliquots over 48 hours. We subsequently used liquid-chromatography high-resolution mass spectrometry (LC-HRMS) to measure the relative amounts of **1a**–**b**, the partially decaged derivative where one of the caging groups on the β-phosphate has been hydrolyzed (**3a**–**b**), and fully released IPP (Figure 3A–B). The observed reduction of **1a** and **1b** indicates that *B. subtilis* can hydrolyze the esters of both hexanoate and pivaloate derivatives beyond background hydrolysis (Figure S2). Interestingly, we found that the rate of cleavage of the first ester protected side chain is similar for both compounds. This is contrary to the *p*-nitrophenyl ester assay, which demonstrated rapid hydrolysis of the hexanoate ester but limited hydrolysis of the pivaloate ester. Furthermore, as demonstrated in Figure 3A, the esterase catalyzed hydrolysis of **3b** is slow when compared to **3a** at 24 h. This result is supported by the previous work by Meier et al., demonstrating that cleavage of the second ester is slower due to the negative charge of the mono-protected pyrophosphate; however, *B. subtilis* possesses sufficient esterase activity for uncaging of **1a** to IPP or DMAPP on a time scale that is consistent with feeding assays.[30] It is important to highlight that the cleavage rate observed in our experiment may not reflect the actual rate within *B. subtilis* cells, given that the protein concentration *in vivo* likely varies from the 100 ng/μL used in our experimental method. In addition, the cleavage of **1a** and **1b**, which are SIEs of IPP, rather than a model compound also highlights the limitations of the *p*-nitrophenyl ester assay, which serves merely as in indicator of esterase activity due to the fixed nitrophenyl ester linkage. The *p*-nitrophenyl ester assay did, however, correctly indicate that the straight chain hexanoate ester would be hydrolyzed more rapidly than the pivalolate ester derivative. Once we established that **1a** and **2a** were viable candidates for cellular delivery to *B. subtilis*, we sought to evaluate whether the SIE strategy was potentially toxic due to the release of caproic acid and *p*-quinone methide.

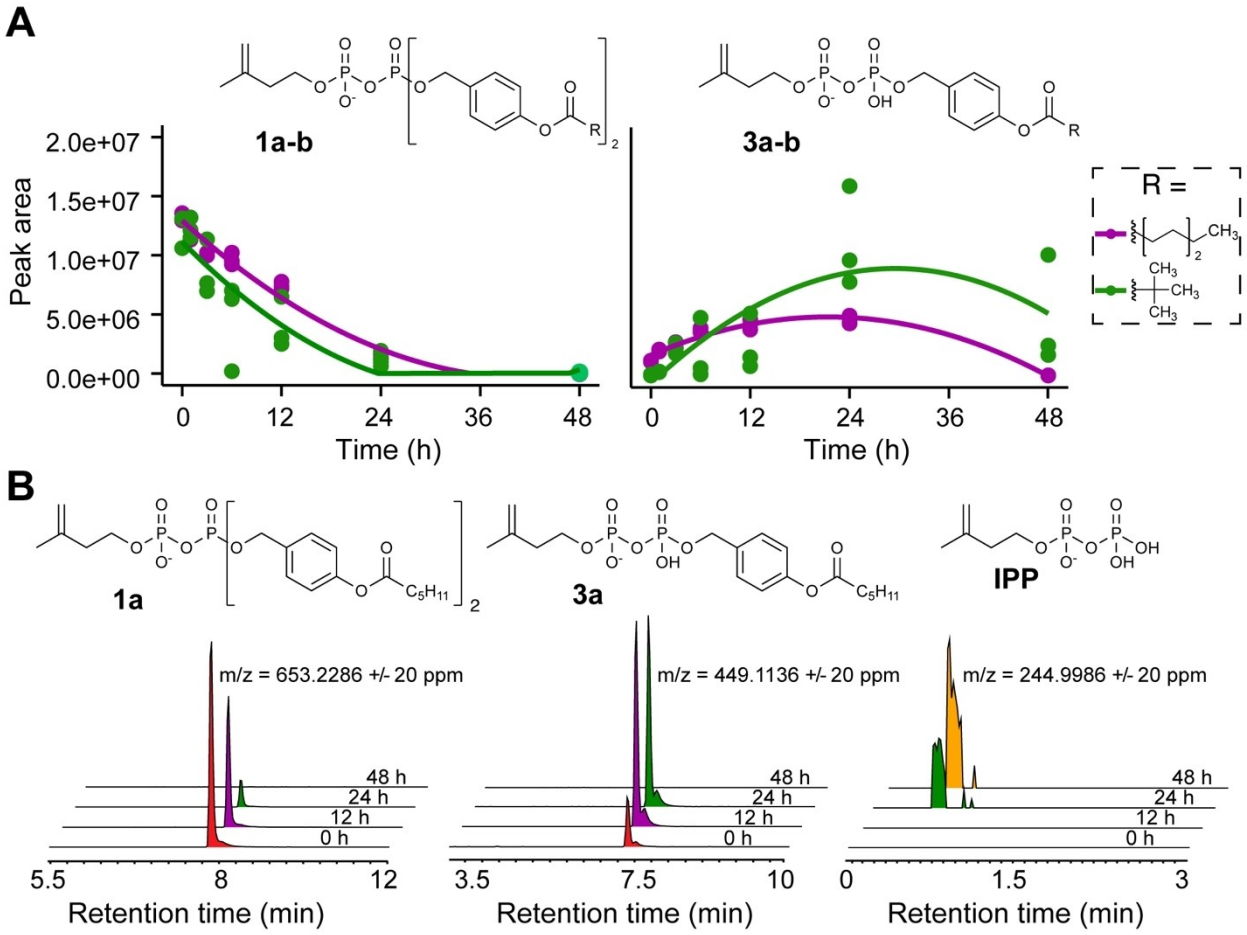

Figure 3. LC-HRMS analysis of *B. subtilis* lysates incubated with 1 a and 1 b. (A) The LC-HRMS peak area of **1 a**–**b** and **3a**–**b** demonstrating loss of **1 a**–**b** over 48 h. N = 3 **(B)** Extracted-ion-chromatograms (EICs) for **1 a**, **3 a** and IPP at 0 h, 12 h, 24 h, and 48 h, of incubation with *B. subtilis* lysate.

Examination of Potential Toxicity From the SIE Delivery Strategy for Cell-Permeant IPP and DMAPP Analogs in *B. Subtilis*

To establish the viability of our SIE delivery approach, we set out to measure the change in growth of *B. subtilis* with the administration of our SIE-caged pyrophosphates without the delivery of IPP or DMAPP. First, we aimed to establish the inhibitory concentration of **1 a** and **2 a**, defined as a reduction in growth to less than 10% of the control, as measured by the area under the growth curve of continual OD 600 measurements on a plate reader. We demonstrated both **1 a** and **2 a** inhibit the growth of *B. subtilis* when administered at concentrations at or above 500 μM (Figure 4A, Figure 4D, Figure S3A). It has previously been difficult to assess the relative toxicity of IPP as compared to DMAPP. Our finding that both isomers generate toxicity at comparable doses is of critical importance when designing strategies to mitigate IPP and DMAPP toxicity, particularly for metabolic engineers attempting to boost yields of isoprenoids. One obvious concern related to the observed inhibitory concentrations of **1 a** and **2 a** is that it was caused in part or completely by the released caging group, rather than by IPP or DMAPP. Therefore, we investigated the effects of caproic acid and generation of *p*-quinone methide that results from the SIE-caging strategy on the growth of *B. subtilis*.

To generate both caproic acid and *p*-quinone methide in *B. subtilis*, we synthesized an SIE-caged pyrophosphate of isopentanol (**4**) as a control compound, which possesses the same ester functionality but lacks the bioactivity of IPP or DMAPP due to being fully saturated (Figure 4B, Scheme S2). Only at concentrations exceeding 500 μM of **5** did we notice a reduction in the growth curve of *B. subtilis* and at no concentration tested did growth fall below 60% of the vehicle control (Figure 4C–D). Collectively, the lack of reduction in growth from **4** compared to **1 a** and **2 a** indicates that the adverse growth effects observed at and above 500 μM of **1 a** and **2 a** result from the introduction of IPP or DMAPP and not caproic acid or *p*-quinone methide. The behavior of **4** not only clarifies the safety profile regarding the release of IPP and DMAPP but also sheds light on the broader context of *p*-quinone methide release from SIE analogs used in *B. subtilis*. Our evaluation of the toxicity of the SIE delivery method for IPP and DMAPP demonstrates that there is significant tolerance towards caging group by-products such as caproic acid and *p*-quinone methide, underscoring its potential broad applicability in bacteria.

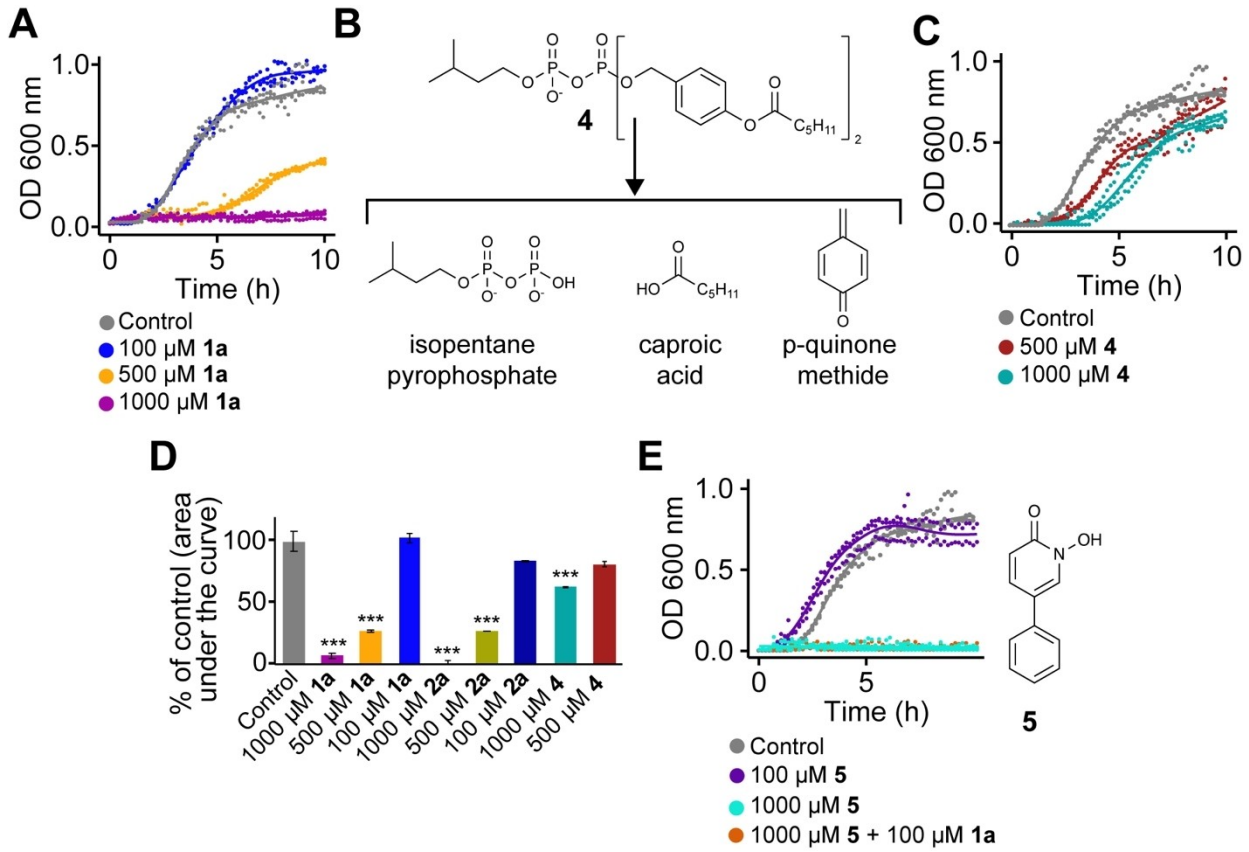

Figure 4. Assessment of *B. subtilis* growth after addition of exogenous IPP, 4, or 5 as determined by OD 600. **(A)** Treatment of *B. subtilis* with **1 a**. **(B) 5** allows for the *in-situ* production of inert isopentanol pyrophosphate, caproic acid, and *p*-quinone methide. **(C)** Treatment of *B. subtilis* with **4**. **(D)** Deviation from control was determined by the area under the growth curve shown in **A**, **C**, and Figure S3A. **(E)** Treatment of *B. subtilis* with **5** with and without the addition of **1 a**. N = 3

Determining the Bioavailability of Cell-Permeant Analogs of IPP and DMAPP

Once we established the necessary ester composition to enable IPP and DMAPP release in *B. subtilis* and eliminated concerns of off-target effects associated with uncaging of the pyrophosphate, we set out to demonstrate that uncaging of **1 a** and **2 a** results in bioavailable IPP and DMAPP. Specifically, we wanted to demonstrate that the release of IPP and DMAPP would allow bacterial growth even with complete inhibition of the endogenous IPP and DMAPP source, the MEP pathway. To inhibit the MEP pathway, we first pursued a phenylpyridinone-based inhibitor (**5** Figure 4E), which was reported to be an inhibitor of 1-deoxy-D-xylulose 5-phosphate reductoisomerase (DXR).[31] We synthesized **5** via a modified procedure from the previously reported method by the Yongchen lab (Scheme S3). With **5** at our disposal, we administered it to the media of *B. subtilis* cultures at concentrations of 100 uM and 1 mM and monitored growth, as described above. We observed insignificant reduction in growth at 100 uM and complete growth inhibition at 1 mM of **5**; however, we did not observe rescue when we co-administered our cell-permeant IPP (**1 a**) or DMAPP (**2 a**) (Figure 4E). One potential explanation for the lack of rescue is that **5** is nonspecific to the DXR enzyme and is inhibiting other essential enzymes that prevent the growth of *B. subtilis*. Given that **5** has not previously been validated *in vivo*, we turned to fosmidomycin, which is a well-established specific inhibitor of the DXR enzyme.

Fosmidomycin initially seemed like an impractical choice, due to its lack of inhibition to Gram positive bacteria. However, we found that at concentrations greater than 1 mM of fosmidomycin there was complete inhibition *B. subtilis* growth (Figure S4). These results suggest that fosmidomycin does act as a MEP pathway inhibitor in *B. subtilis*; therefore, we moved forward to attempt rescuing the MEP pathway using **1 a** and **2 a.**

To demonstrate the rescue of growth after treatment with fosmidomycin, we added **1 a** or **2 a** at concentrations of 10, 50, and 100 μM. We observed dose dependent rescue with the addition of **1 a** (Figure 5A, 5B, and 5 C). In contrast, adding IPP without SIE-caging of the β-phosphate did not result in rescued cell growth during coadministration with fosmidomycin (Figure S5). While some bacteria are capable of transporting IPP into the cell, in *B. subtilis* the lack of rescued growth clearly demonstrates the need for cell-permeant analogs of IPP and DMAPP. Similarly, **1 b** and **2 b** were not able to rescue the growth of *B. subtilis*, which was unexpected given that we previously demonstrated that they are uncaged in the presence

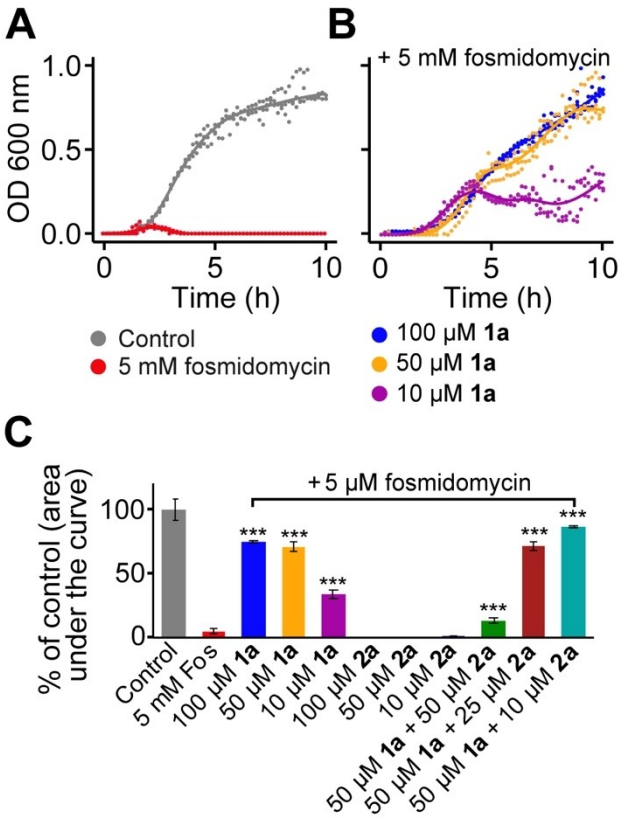

Figure 5. Assessment of *B. subtilis* growth after addition of exogenous IPP and DMAPP as determined by OD 600. **(A)** *B. subtilis* with vehicle control and treatment with 5 mM fosmidomycin, **(B)** Treatment with 5 mM fosmidomycin with concurrent addition of **1a**. **(C)** Deviation from control was determined by the area under the growth curve after treatment with fosmidomycin derived from growth curves shown in **A**–**B** and Figure S3B–C. N = 3.

of *B. subtilis* lysates, albeit at a slower rate than **1a** and **2a** (Figure 3A-B, Figure S6). We interpreted this discrepancy as **1b** is hydrolyzed to **3b** but not IPP in *B. subtilis* or that the pivaloate group does not render these IPP or DMAPP analogs non-polar enough to enable them to pass through the cell membrane. Unexpectedly, **2a** also did not rescue the growth of *B. subtilis* after treatment with fosmidomycin at any concentration tested (Figure 5C, Figure S3B). We hypothesize this is either due to the high concentrations of fosmidomycin creating off target effects that do not allow for rescue of DMAPP alone, or low expression of the isopentyl pyrophosphate isomerase (IPPI) expressed in *B. subtilis*, which would be necessary to convert DMAPP into IPP for both substrates to be present when the DXR enzyme is inhibited.

We then set out to identify the optimal ratio of IPP to DMAPP that would facilitate *B. subtilis* growth under MEP pathway inhibition by high concentrations of fosmidomycin. With co-administration of fosmidomycin, we added **1a** and **2a** in a 1:1, 2:1, and 5:1 ratio and then measured the growth curve of *B. subtilis* over 10 h (Figure 5C, Figure S3C). We observed that the growth curve of *B. subtilis* most closely resembled the vehicle control at a 5:1 ratio of **1a** to **2a**. Interestingly, the 5:1 ratio of IPP and DMAPP delivered to *B. subtilis* by **1a** and **2a** mirrors the 5:1 IPP and DMAPP ratio produced (E)-4-hydroxy-3-methylbut-2-enyl diphosphate reductase (HDR), the last enzyme in the MEP pathway.[32]

Conclusions

In this study, we show that cell-permeant analogs of IPP and DMAPP are viable chemical tools for studying the isoprenoid pathway in *B. subtilis*. We began this work by initial selection of the appropriate ester for β-phosphate caging that would enable cell entry and subsequent release in *B. subtilis*. We optimized the composition of our SIE and demonstrated that *B. subtilis* possesses native esterases that favor straight chain substrates using a *p*-nitrophenyl ester assay and a comprehensive LC-HRMS analysis of **1a**–**b** incubated in *B. subtilis* lysates. We demonstrated that the SIE delivery strategy contributes minimally to the growth of *B. subtilis* via a toxicity comparison of **1a** and **2a** against a new control compound, **5**. This finding shows that both IPP and DMAPP are toxic metabolites at elevated concentrations, which means altering the ratio of IPP and DMAPP inside the cell will not alleviate a toxic phenotype potentially encountered during metabolic engineering of the MEP pathway. Finally, we established that our cell-permeant analogs yield bioavailable IPP and DMAPP, which we have demonstrated by MEP pathway inhibition followed by the rescue of growth by **1a** in a dose dependent manner. Additionally, we found that a five to one ratio of IPP to DMAPP resulted in optimal growth of *B. subtilis* after treatment with fosmidomycin, and that, surprisingly, rescue could be achieved with IPP alone but not with DMAPP alone. These findings not only demonstrate the effectiveness of SIE-caging for exogenous delivery of IPP and DMAPP in *B. subtilis* but also provide valuable insights into the distinct demands for these isomers, which has significant implications for metabolic engineering research targeting isoprenoid production and broadens the potential applications of SIE-caging in the exploration of the chemical biology of bacteria.

Experimental Procedures

General

All chemicals were purchased from either Fisher Scientific or Millipore Sigma and used without purification. Dry solvents were prepared by distillation and storage over 3 Å molecular sieves. All reactions unless indicated were carried out in flame-dried glassware under argon. Argon was dried by passing through calcium sulfate. Thin-layer chromatography (TLC) was performed using either Baker-flex® disposable TLC plates (J.T. Baker) or TLC Silica gel 60 F_{245} glass-backed TLC plates (Millipore Sigma). Visualization was achieved either using UV light (254 nm) and/or staining in $KMnO_4$ (1 g $KMnO_4$, 6.67 g K_2CO_3, 1.67 mL 5% NaOH in 100 mL of H_2O). Flash chromatography of crude products was performed using a Buchi Pure C-850

FlashPrep chromatography system with pre-packed silica or C18 cartridges where indicated.

NMR Spectroscopy

^{1}H, ^{13}C, and ^{31}P spectra were recorded on a Bruker Ascend 500 (500 MHz) with a Bruker 5 mm BBFO SmartProbe with indicated solvents used as the internal deuterium lock. All chemical shifts are reported in ppm spectra are referenced using the residual solvent peak. ^{31}P NMR spectra are decoupled from proton signal.

The multiplicity of reported signals is indicated as followed: s (singlet), d (doublet), dd (doublet of doublets), t (triplet), q (quartet), m (multiplet). The number (n) of protons represented by each signal is denoted as nH. The coupling constants were determined by analysis using Mestrenova software (version 14.3.0) and reported to the nearest 0.01 Hz.

Bacterial Culturing

Bacillus subtilis 6051 and *Escherichia coli* DH10b were obtained from ATCC (Manassas, VA). For all experiments, cells were isolated from single colonies grown on Luria-Bertani (LB) agar incubated at 37 °C. Liquid cultures were maintained in LB broth and incubated in a shaking incubator at 250 rpm at 37 °C.

Bacterial Growth Curves

Into a microcentrifuge tube in triplicate, the compound(s) of interest were combined with LB broth and either *B. subtilis* or *E. coli*, which was grown to an OD600 of 1 then was added to the triplicate at a 20x dilution of the culture. The mixture was then briefly vortexed to ensure a homogonous mixture and then transferred into a 96 well plate. Next, the OD600 of the 96 well plate was measured by the Cytation 1 cell imaging multimode microplate reader with OD600 measurments taken every 10 min for 10 h at 37 °C with orbital shaking at 528 cycles per minute (cpm). All data was baseline corrected and graphs were created using a custom code in R that can be found on GitHub: https://github.com/dmcbee1/Bacillus-Paper

Liquid-Chromatography High-Resolution Mass Spectrometry (LC-HRMS)

LC-HRMS analysis was performed using an Agilent 6530 mass spectrometer coupled to an Agilent 1290 Infinity UHPLC. Separations were carried out under the following chromatographic conditions using an Agilent Poroshell HPH C18 column (2.7 μm, 100×2.1 mm) operating at a flow rate of 0.3 mL/min.

– Liquid Chromatography (LC) Conditions:
  - Mobile Phase:
  - Solvent A: 0.1 % Ammonium hydroxide in water.
  - Solvent B: 50 % methanol / 50 % acetonitrile.
  - Gradient Program:
  - 0–1 min: 100 % A.
  - 1–11 min: Linear gradient from 100 % A to 100 % B.
  - 11–13 min: Hold at 100 % B.
  - 13–15 min: Return to initial conditions (100 % A).
  - Column Temperature: 40 °C.
  - Injection Volume: 1 μL.
– Quadrupole Time-of-Flight (QTOF) Mass Spectrometry Conditions:
  - Polarity: Negative ion mode.
  - Flow Path:
  - 0–0.5 min: Diverted to waste
  - 0.5–13 min: Directed to the mass spectrometer.
  - Post 13 min: Diverted to waste.
  - Gas Parameters:
  - Gas Temperature: 325 °C.
  - Nebulizer Pressure: 25 psig.
  - Sheath Gas Temperature: 350 °C.
  - Sheath Gas Flow Rate: 12 L/min.
  - VCap Voltage: 3500 V.
  - Acquisition Mode: Mass Spectrometry (MS), Extended Dynamic Range
  - Mass Range: 100–1700 m/z.

LC-HRMS B. Subtilis Lysate Assay

A 50 mL culture of *B. subtilis* was grown overnight in Luria-Bertani (LB) broth at pH 7.5. This culture was transferred to a 50 mL conical vial and centrifuged at 3,000×g for 10 min at 4 °C. The supernatant was removed and the pellet was resuspended in ice cold 0.9 % NaCl in ultra-pure water (Milli-Q IQ 7000, Millipore-Sigma). This process was repeated for a total of three washing steps. The bacterial pellet was then resuspended in 15 mL Tris buffer (10 mM Tris-HCl, 100 mM NaCl, 0.5 % Tween-80, pH 7.5) and then sonicated (Fisherbrand model 505 sonic dismembrator, Fisher Scientific) on ice at 40 % intensity with a 2 sec pulse for a total sonication time of 2 min. The lysate was then clarified by centrifugation at 18,000×g for 15 min at 5 °C. The clarified supernatant was then transferred to a conical vial and protein concentration was determined by Bradford assay. The Bradford assay was done as described by ThermoFisher and was conducted in a 96 well plate. Next, protein concentration was normalized to 100 ng/μL in 10 mM Tris buffer and filtered through a 0.22 μM filter to ensure sterility.

Created in triplicate, 1 mL of either Tris buffer alone or the *B. subtilis* lysate was added to a 1.5 mL conical vial. Next, 1 μL of a 100 mM stock of either **1a** or **1b** were added to their respective triplicate, making a 100 μM working concentration. The conical vials were sealed and incubated at 37 °C on a heat block (Thermomixer C, Eppendorf) and 10 μL aliquots were taken at 0, 1, 3, 6, 12, 24, and 48 h. Each aliquot was mixed with 90 μL of methanol and then centrifuged at 18,000×g for 10 min at 5 °C. All aliquots were taken near a flame for sterility. The supernatant was then transferred to a LC/HRMS vial and immediately analyzed using LC/HRMS. Extracted ion chromatograms (EICs) were extracted using MassHunter Qualitative

Analysis software (Agilent). EICs were graphed relative to the 0 h timepoint of **1a** or **4a** and to 48 h for IPP. Quantitation of each EIC was completed using MassHunter Quantative Analysis (Agilent) and all graphs were generated using custom R code (GitHub: https://github.com/dmcbee1/Bacillus-Paper).

Author Contributions

Dillon P. McBee: Conceptualization; data curation; formal analysis; methodology; software; writing – original draft preparation; writing – review & editing. **Zackary N. Hulsey**: Data curation; methodology; writing – review & editing. **Makayla R. Hedges**: Data curation; methodology; writing – review & editing. **Joshua A. Baccile**: Conceptualization; funding acquisition; project administration; supervision; visualization; writing – review & editing.

Acknowledgements

This work was supported by the National Science Foundation Chemistry of Life Processes (NSF-CLP) program (CHE-2204170). The authors would like to thank Dr. Francis Rossi of the State University of New York at Courtland for his useful conversations and helpful feedback.

Conflict of Interests

There are no conflicts to declare.

Data Availability Statement

All data is available upon request from Joshua A. Baccile jbaccile@utk.edu.

[1] P. A. Edwards, J. Ericsson, *Annu. Rev. Biochem.* **1999**, *68*, 157–85.
[2] J. Grünler, J. Ericsson, G. Dallner, *Biochim. Biophys. Acta* **1994**, *1212*, 259–277.
[3] J. L. Goldstein, M. S. Brown, *Nature* **1990**, *343*, 425–30.
[4] A. Banerjee, T. Sharkey, *Nat. Prod. Rep.* **2014**, *31*, 1043–1055.
[5] J. C. Sacchettini, C. D. Poulter, *Science* **1997**, *277*, 1788–1789.
[6] D. W. Christianson, *Science* **2007**, *316*, 60.
[7] F. Pietrocola, L. Galluzzi, J. M. B. S. Pedro, F. Madeo, G. Kroemer, *Cell Metab.* **2015**, *21*, 805–21.
[8] H. M. Miziorko, *Arch. Biochem. Biophys.* **2011**, *505*, 131–43.
[9] Y. Hoshino, E. A. Gaucher, *Mol. Biol. Evol.* **2018**, *35*, 2185–2197.
[10] P. A. Konstantinopoulos, M. V. Karamouzis, A. G. Papavassiliou, *Nat. Rev. Drug Discovery* **2007**, *6*, 541–555.
[11] S. Shack, M. Gorospe, T. W. Fawcett, W. R. Hudgins, N. J. Holbrook, *Oncogene* **1999**, *18*, 6021–6028.
[12] J. D. Rudolf, T. A. Alsup, B. Xu, Z. Li, *Nat. Prod. Rep.* **2021**, *38*, 905–980.
[13] N. N. Gerber, *Tetrahedron Lett.* **1968**, *9*, 2971–2974.
[14] J. S. Dickschat, H. B. Bode, T. Mahmud, R. Müller, S. Schulz, *J. Org. Chem.* **2005**, *70*, 5174–5182.
[15] A. Nakagawa, Y. Iwai, H. Hashimoto, N. Miyazaki, R. Oiwa, Y. Takagashi, A. Hirano, N. Shibukawa, Y. Kojima, S. Omura, *J. Antibiot.* **1981**, *34*, 1408–1415.
[16] M. J. Smanski, R. M. Peterson, S. R. Rajski, B. Shen, *Antimicrob Agents Chemother.* **2009** *53*, 1299–1304.
[17] X. Pan, J. D. Rudolf, L. B. Dong, *Nat. Prod. Rep.* **2024**.
[18] Y. Zhang, L. M. Prach, T. E. O'Brien, F. DiMaio, D. M. Prigozhin, J. E. Corn, T. Alber, J. B. Siegel, D. J. Tantillo, *Biochemistry.* **2020**, *59*, 4507–4515.
[19] E. J. N. Helfrich, G. M. Lin, C. A. Voigt, J. Clardy, *Beilstein J. Org. Chem.* **2019**, *15*, 2889–2906.
[20] D. E. Cane, H. Ikeda, *Acc. Chem. Res.* **2012**, *45*, 463–472.
[21] N. Ziemert, M. Alanjary, T. Weber, *Nat. Prod. Rep.* **2016**, *33*, 988–1005.
[22] J. Kuzma, M. Nemecek-Marshall, W. H. Pollock, R. Fall, *Curr. Microbiol.* **1995**, *30*, 97–103.
[23] B. Erickson, Nelson, P. Winters, *Biotechnol. J.* **2012**, *7*, 176–185.
[24] S. C. Phulara, P. Chaturvedi, P. Gupta, *Appl. Environ. Microbiol.* **2016**, *82*, 5730–5740.
[25] K. W. George, M. G. Thompson, J. Kim, E. E. K. Baidoo, G. Wang, V. T. Benites, C. J. Petzold, L. J. G. Chan, S. Yilmaz, P. Turhanen, P. D. Adams, J. D. Keasling, T. S. Lee, *Metab. Eng.* **2018**, *47*, 60–72.
[26] H. Mönkkönen, S. Auriola, P. Lehenkari, M. Kellinsalmi, I. E. Hassinen, J. Vepsäläinen, J. Mönkkönen, *Br. J. Pharmacol.* **2006**, *147*, 437–445.
[27] F. M. Rossi, D. P. McBee, T. N. Trybala, Z. N. Hulsey, C. G. Curbelo, W. Mazur, J. A. Baccile, *ChemBioChem* **2023**, *24*, e202200512.
[28] K. Blank, J. Morfill, H. Gumpp, H. E. Gaub, *J. Biotechnol.* **2006**, *125*, 474–83.
[29] C. Huggins, J. Lapides, *JBC* **1947**, *170*, 467–482.
[30] X. Jia, D. Schols, C. Meier, *J. Med. Chem.* **2020**, *63*, 6003–6027.
[31] L. Deng, S. Sundriyal, V. Rubio, Z. Shi, Y. Song, *J. Med. Chem.* **2009**, *52*, 6539–6542.
[32] D. C. Volke, J. Rohwer, R. Fischer, et al. *Microb. Cell Fact.* **2019**, *18*, 192.

Manuscript received: January 23, 2024
Revised manuscript received: March 28, 2024
Accepted manuscript online: April 3, 2024
Version of record online: April 24, 2024